LA-UR-17-23390
Approved for public release; distribution is unlimited.

Title: Final Project Report: Imaging Fault Zones Using a Novel Elastic Reverse-Time Migration Imaging Technique

Author(s): Huang, Lianjie

Intended for: Report

Issued: 2017-05-10 (rev.1)

Final Report

LANL Project Number: 0522-1589

Imaging Fault Zones Using a Novel Elastic Reverse-Time Migration Imaging Technique

PI: Lianjie Huang

Team Members: Lianjie Huang, Ting Chen, Sirui Tan, Youzuo Lin, and Kai Gao

Los Alamos National Laboratory
Geophysics Group, MS D452
Los Alamos, NM 87545

Industry Collaborator: Magma Energy (U.S.) Corp.

DOE-GTO Program Managers: Eric Hass, Mark Ziegenbein, Brittany Segneri, and Holly Thomas

Acknowledgements:

This work was supported by the Geothermal Technologies Office (GTO) of the U.S. Department of Energy through contract DE-AC52-06NA25396 to Los Alamos National Laboratory. We thank strong support of GTO Program Managers Eric Hass, Mark Ziegenbein, Holly Thomas, and Brittany Segneri. We thank Holly Thomas for her careful review of this report and her valuable comments. We thank George Guthrie and David Coblentz of LANL for their help in preparing and reviewing this report. We thank Magma Energy (U.S.) Corp for providing us with raw seismic data acquired at the Soda Lake geothermal field. The computation was performed using supercomputers of LANL's Institutional Computing Program.

(Los Alamos Unlimited Release Number: LA-UR-17-23390)

Contents

1 Executive Summary

Imaging fault zones and fractures is crucial for geothermal operators, providing important information for reservoir evaluation and management strategies. However, there are no existing techniques available for directly and clearly imaging fault zones, particularly for steeply dipping faults and fracture zones. In this project, we developed novel acoustic- and elastic-waveform inversion methods for high-resolution velocity model building. In addition, we developed acoustic and elastic reverse-time migration methods for high-resolution subsurface imaging of complex subsurface structures and steeply-dipping fault/fracture zones. We first evaluated and verified the improved capabilities of our newly developed seismic inversion and migration imaging methods using synthetic seismic data. Our numerical tests verified that our new methods directly image subsurface fracture/fault zones using surface seismic reflection data. We then applied our novel seismic inversion and migration imaging methods to a field 3D surface seismic dataset acquired at the Soda Lake geothermal field using Vibroseis sources. Our migration images of the Soda Lake geothermal field obtained using our seismic inversion and migration imaging algorithms revealed several possible fault/fracture zones. AltaRock Energy, Inc. is working with Cyrq Energy, Inc. to refine the geologic interpretation at the Soda Lake geothermal field. Trenton Cladouhos, Senior Vice President R&D of AltaRock, was very interested in our imaging results of 3D surface seismic data from the Soda Lake geothermal field. He planed to perform detailed interpretation of our images in collaboration with James Faulds and Holly McLachlan of University of Nevada at Reno. Using our high-resolution seismic inversion and migration imaging results can help determine the optimal locations to drill wells for geothermal energy production and reduce the risk of geothermal exploration.

2 Overview of the Project Research

The Challenge

Fault zones can control the flow paths of hot water in hydrothermal geothermal systems, and they often confine the boundaries of the reservoir. Moreover, faults and fractures are the primary flow pathways in fracture-dominated reservoirs. Hence, imaging fault zones and fractures is crucial for geothermal operators, providing important information for reservoir evaluation and management strategies.

However, there are no existing techniques available for directly and clearly imaging fault zones, particularly for steeply dipping faults and fracture zones. In this project, we developed and evaluated a new methodology that uses surface seismic reflection data to produce 3D images and a 3D velocity model to reveal features in vertically oriented fault/fracture zones. We demonstrated this new methodology using both synthetic and real seismic datasets, illustrating the improved imaging results using 2D and 3D seismic images and velocity models produced using newly developed seismic-waveform inversion and migration imaging algorithms.

Limitations of Current Standard Methods Relative to the Challenge

Conventional seismic imaging, called prestack time migration, uses a one-dimensional (1D) velocity model to stack seismic data and to form an image in the time domain instead of in the space domain. Such images have a poor image resolution so the interpretation of fault zones is often subjective.

Current state-of-the-art seismic imaging provides a significant improvement in resolution over conventional imaging, but vertically oriented features remain poorly resolved. State-of-the art imaging in industry is based on reverse-time migration using 2D/3D velocity models obtained from migration velocity analysis. This imaging technique produces images in the space domain. Its image resolution is higher than that of time-domain images produced using prestack time migration. However, the resolution of the velocity models from migration velocity analysis is still low, and the resulting images mainly show the layered sedimentary layers.

Hypothesis and Proposed Research to Overcome the Challenge

The goal of this project was to overcome the challenge of imaging steeply-dipping fault zones by developing and evaluating two new methodologies for processing seismic data. Our hypothesis is that additional and important information on the features of interest is contained in seismic data collected at a geothermal site, but this information is not properly used in conventional seismic imaging approaches, including conventional seismic inversion to produce a velocity model and conventional migration imaging. We further hypothesize that this information can be extracted to provide useful interpretations by exploiting: (a) full seismic waveforms (as opposed to simply major reflections) and (b) a new imaging method, called reverse-time migration imaging with separated wavefields. In this project, we tested these hypotheses using two approaches.

First, we developed a suite of novel acoustic- and elastic-waveform inversion methods to build a high-resolution velocity model for use with reverse-time migration. The velocity model is a central input into seismic migration imaging techniques, providing a "best guess" of subsurface geophysical properties that control seismic-wave propagation and back-propagation used in seismic migration imaging. In conventional approaches, a velocity model is based on combination of: (1) a site-geologic model developed from an geologic interpretation of the site's subsurface, and (2) an inversion of seismic data using primary signals in the waveform (e.g., arrival times of seismic reflections). In the latter case, the primary signals contain minimal information on vertically oriented features. However, the entire seismic waveform does contain information on the features of interest, but the information is not simple to extract (as in the case of seismic reflections). Hence, we focused on developing an inversion method that produces a velocity model using the entire seismic waveform. In this effort, we developed the algorithms needed to conduct the inversion.

Second, we developed a suite of novel acoustic- and elastic-wave reverse-time migration methods to produce images that contain information on both horizontal and vertical features, utilizing the velocity model produced by full-waveform inversion. Our methodology first produces conventional downward-looking migration images, which show detail on horizontal features. Then we produce lateral-looking migration images that reveal steeply-dipping features (like fault zones). Finally, we combine the downward-looking migration image with the lateral-looking migration im-

age to form a high-resolution migration image that contains both horizontal and vertical structure information. We developed two versions of the reverse-time imaging methods: our acoustic-based inversion and migration imaging methods can be applied to imaging with one-component seismic data; our elastic-based inversion and migration imaging methods can be applied to imaging with multi-component seismic data.

We demonstrated using synthetic and field seismic data from the Soda Lake geothermal field that LANLs newly developed acoustic- and elastic-waveform inversion and reverse-time migration methods have great potential to clearly image subsurface fracture/fault zones using surface seismic reflection data.

Our Approach and Detailed Developments

Our work involved three general steps.

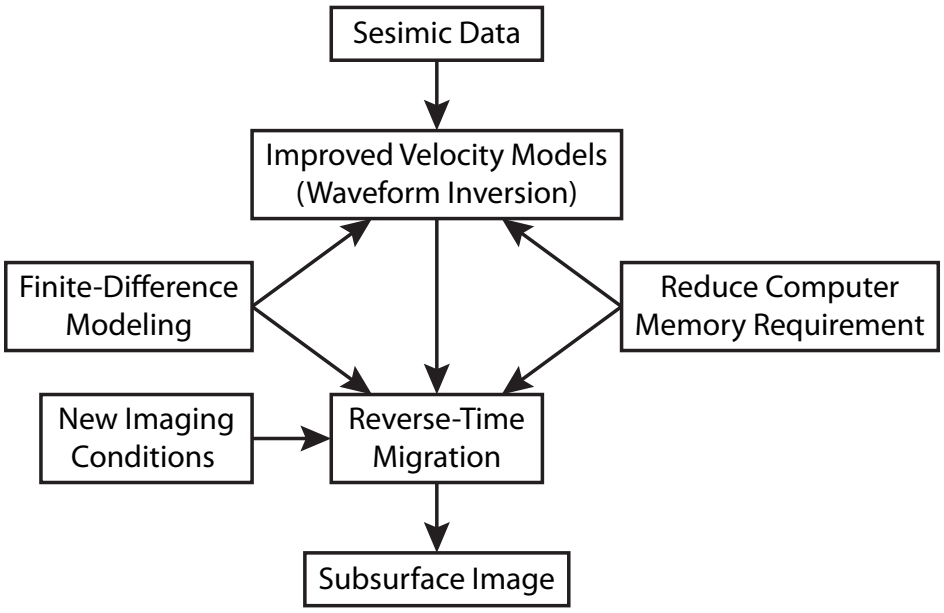

Figure 1: Relationship among research topics for the project.

First, we developed and implemented our new 2D and 3D algorithms for both full-waveform inversion and reverse-time migration imaging. The overall workflow for this process is shown in Fig 1. Second, we validated and refined these algorithms using synthetic seismic datasets for a geophysical model built using the geologic features found at the Soda Lake geothermal field. Finally, we applied our new seismic full-waveform inversion and reverse-time migration imaging algorithms to a 3D seismic dataset acquired at the Soda Lake geothermal field, and revealed several possible fault/fracture zones.

In the first step, we addressed two challenges. First, we developed new algorithms necessary for both full-waveform inversion and reverse-time migration. Then, to make these techniques practical for non-research users, we optimized the algorithms with respect to speed and memory requirements. Specific outcomes include:

1. A novel finite-difference seismic-wave modeling method that is used both in full-waveform inversion and reverse-time migration. Our new algorithm is approximately two times more computationally efficient than conventional finite-difference modeling methods.
2. A novel method to reduce computer memory requirement for seismic-wavefield backpropagation, a key step in both reverse-time migration and full-waveform inversion. Our new method uses only 37.5% of the computer memory required by a most commonly used method.
3. Novel full-waveform inversion methods using acoustic- (single component) and elastic-wavefields (multiple components) to obtain improved velocity models needed for accurate reverse-time migration imaging. Our new methods can build more accurate, higher-resolution velocity models with sharp interfaces than conventional methods.

In the second step, we demonstrated our algorithms using synthetic seismic datasets. We also used these synthetic datasets to refine the methodology for application to real datasets. Specific outcomes include:

4. Novel imaging conditions for reverse-time migration. Our method first separates the forward-propagating source wavefield and the backward-propagating receiver wavefield into left- and right-going (or down-going and up-going) waves and then applies the Poynting-vector imaging condition to the separated wavefields. By separating the wavefields, we significantly improved the accuracy of reverse-time migration imaging in complex regions.
5. Novel reverse-time migration methods to improve migration images. We developed least-squares reverse-time migration methods that use the wavefield-separation imaging condition and updated source wavefield along with modified total-variation regularization. This new methodology significantly improves imaging of steeply-dipping fault zones and reduces migration artifacts.

In the final step, we tested our algorithms by application to field seismic data from the Soda Lake geothermal field. The raw field seismic data were provided by Magma Energy (U.S.) Corp. and we subsequently had the prestack version of the original data re-processed by Vecta Oil & Gas, Ltd., resulting in a dataset that included full seismic waveforms for 8317 common-shot gathers, or 2972 common-receiver gathers. We used this final set of seismic waveforms with our new seismic inversion and reverse-time migration imaging algorithms to produce both a velocity model and a migration image. Specific outcomes include:

6. Application of 3D full-waveform inversion and 3D reverse-time migration to the 3D surface seismic data acquired at the Soda Lake geothermal field. We produced compression-to-compression (PP) images and compression-to-shear (PS) converted-wave images using our new methodology and compared these results to results obtained from current state-of-the-art imaging methods.

Does the New Imaging Methodology Provide Improved Information on Vertical Features?

We highlight the effectiveness of the new methodologies using examples from both seismic synthetic datasets (Figs. 2-3) and a real seismic dataset (Fig. 4).

Figure 2 shows the effectiveness of the new methodology for producing an improved velocity model using full waveform inversion. The examples in Fig. 2 are 2D slices through a full 3D

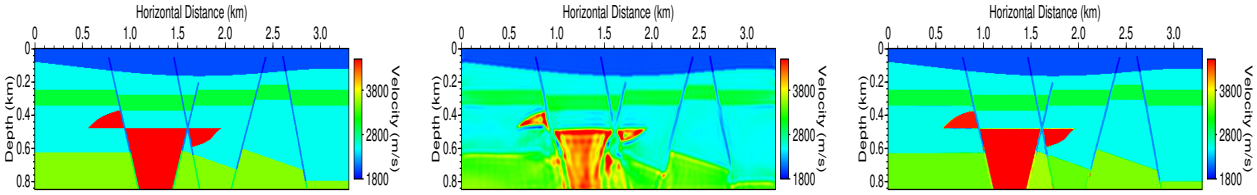

(a) True Velocity Model (b) Conventional inversion (c) LANLs new inversion

Figure 2: Left panel: A velocity model built using geologic features found at the Soda Lake geothermal field; Middle panel: Inverted velocity model obtained using conventional full-waveform inversion; Right panel: Inverted velocity model produced using LANLs new full-waveform inversion method that well reconstructed the sharp interfaces of the basalt bodies in red color and low velocity zones of the faults.

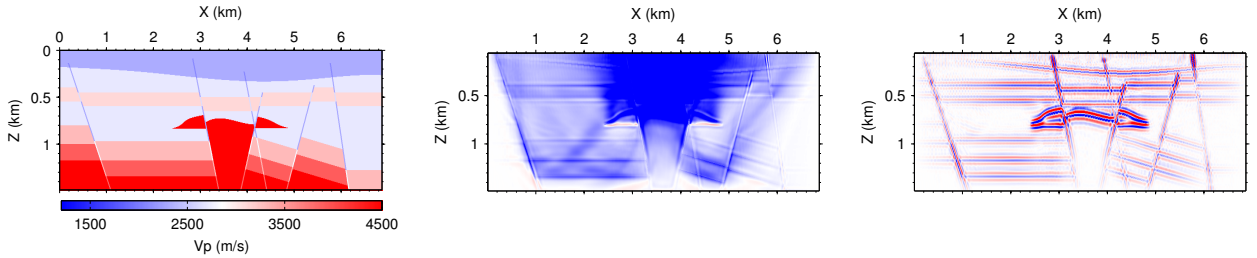

(a) Velocity Model (b) Conventional migration imaging (c) LANLs new migration imaging

Figure 3: Left panel: A Soda Lake geophysical model; Middle panel: Conventional reverse-time migration image; Right panel: LANLs new reverse-time migration image clearly shows steeply-dipping fault zones in addition to the sedimentary layers.

model. This example utilized a synthetic dataset developed for an idealized subsurface geological/geophysical model that was based on the Soda Lake site. The idealized structure (shown in the left panel of Fig. 2) was used to calculate a synthetic seismic dataset that was subsequently used to produce a "calculated" velocity model for the site. We tested the synthetic data in both a conventional inversion approach (middle panel) and in our newly developed seismic full-waveform inversion approach (right panel). As seen in the example, our newly developed seismic full-waveform inversion methodology accurately reconstructed sharp interfaces of basalt bodies and low velocity zones of the idealized site model, and produced a greater level of detail (e.g., higher resolution) than the conventional inversion. This improvement is important in two contexts. First, the new algorithm can extract a higher level of site-specific detail from seismic-waveform data, leading to a better elucidation of the site geology (including vertically oriented features). Second, the improved velocity model represents improved critical input to seismic migration imaging algorithms, including our new reverse-time migration algorithms.

Figure 3 shows the effectiveness of our reverse-time migration algorithm relative to clearly imaging steeply-dipping fault zones. The examples in Fig. 3 are 2D images. This example also utilized a synthetic dataset developed for the idealized subsurface geological/geophysical model from Soda Lake. We used the synthetic data combined with the idealized velocity model (left panel) in our reverse-time migration algorithm. The resulting image (right panel) shows a high level of detail on both horizontal and vertical structure features. This level of detail is a significant

improvement over conventional migration imaging (middle panel), which represents the current state-of-the-art imaging available to industry, in which the background noise can be reduced using filtering after the image is formed.

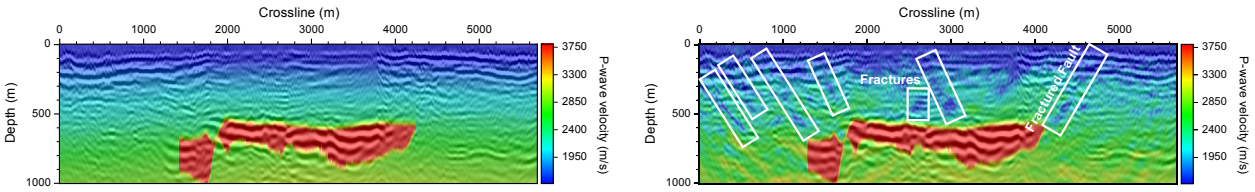

(a) Image on migration analysis velocity model

(b) LANLs new inversion and migration

Figure 4: Comparison between LANLs new full-waveform inversion and reverse-time migration results (right panel) with the state-of-the-art migration result (left panel) for surface seismic data acquired at the Soda Lake geothermal field.

Finally, Fig. 4 shows application of our new methodologies to a real field seismic dataset from the Soda Lake geothermal field. (The examples in Fig. 4 are 2D slices through a full 3D image.) In this example, we used the re-processed field data provided by Vecta Oil & Gas in both of our new methods. First, we obtained two site-specific velocity models using the Soda Lake seismic dataset: one velocity model relied on conventional migration velocity analysis provided by Magma, and it is shown in colored overlay of the left panel in Fig. 4; the other velocity model produced using our new seismic full-waveform inversion methodology, and it is shown as the colored overlay in the right panel of Fig. 4. The underlying images in both of these panels were produced from the Soda Lake dataset using our new reverse-time migration imaging algorithm. Hence, the left-hand panel represents current state-of-the-art velocity model building using the Soda Lake dataset, whereas the right-hand panel illustrates the level of detail achievable with our new seismic full-waveform inversion and reverse-time migration methods. The new methodology clearly shows a higher level of subsurface detail over the state-of-the-art result. Regarding the structural detail, the underlying migration image in Fig. 4(b) shows a high level of detail of subsurface structures, especially overlying the basaltic reservoir (showing as red); note in particular the detail in the region of 2000-4000 m on the crossline, where a high resolution of sedimentary structures is seen. This high level of detail facilitates identification of vertical features (which disrupt the horizontal structure, as shown for example in the boxed areas in the 2600-3000 m region). The most striking improvement, however, is the improved information in the velocity model as extracted from the full seismic waveforms. As shown in the right panel of Fig. 4, the full seismic waveform contains important information on low-velocity zones that are reconstructed and showed as blue. Low velocity regions may correspond to poorly lithified regions of rocks (e.g., gauged fault zones) and/or regions with high fluid content. Some of these vertically-oriented regions are indicated with “boxes” in the right-hand panel of Fig. 4. Although field verification will be an important step in validating the methodologies relative to imaging faults/fractures, this field seismic imaging example demonstrates clearly that the new methodologies can extract significantly more information from seismic datasets than current state-of-the-art methods.

In conclusion, LANLs newly developed acoustic- and elastic-waveform inversion and reverse-time migration methods have great potential to clearly image subsurface fracture/fault zones using surface seismic reflection data.

What Remains to Be Done?

Three next steps have emerged from this work.

One next step is to verify the capabilities of the new seismic imaging methodologies through applications to additional datasets from field sites for which independent details on faults/fractures are already known. Our initial application is promising, but independent verification of the nature of the low velocity zones is unavailable. Ultimately, we need to demonstrate that known faults/fractures can be imaged and that the additional level of information embodied in the new methodology is sufficient to improve field-scale interpretations and decisions.

An additional next step is to extend the methodologies from isotropic to anisotropic, which could significantly improve image details. Sedimentary layers and fracture/fault zones can be strong anisotropic media for seismic-wave propagation. In other words, the properties of the rock differ along different directions through which seismic wave propagates. The research for this project was based on an isotropic assumption, meaning that we did not consider direction-specific properties for the various geologic formations/units in the subsurface, so the anisotropic information contained in the original datasets was not used in the analysis but was instead "averaged" out. This information could improve the reliability of fracture characterization and permeability imaging, but it would be necessary to extend our current isotropic methods to anisotropic seismic-waveform inversion and anisotropic reverse-time migration. These new results could also be integrated with those from other types of geophysical data to produce additional detail on subsurface structures.

Finally, the algorithms developed for this project are research codes. These codes are available for licensing from Los Alamos National Laboratory, but they are tailored to expert users using a Linux-based super-computer platform. Making these readily available to the geothermal community would likely require development of interfaces for non-expert users.

Technical Peer Review

This research resulted in six peer-reviewed journal paper publications, and nine presentations at national and international meetings. Hence, the research is founded in a solid scientific base. The details of the research are contained in the appendices to this final report, which integrate the peer-reviewed publications with the various tasks from the project.

3 Project Objectives of Phase I and Phase II work

Fault zones may control the flow paths of hot water, or confine the boundaries of geothermal reservoirs. Therefore, imaging fault zones is crucial for geothermal exploration and enhanced geothermal systems. However, there are currently no three-dimensional (3D) elastic-migration imaging techniques available for directly and clearly imaging fault zones, particularly for steeply-dipping fault zones.

Prestack depth migration of seismic reflection data is the most robust tool for high-resolution imaging of subsurface structures. Conventional seismic migration uses primary reflections from subsurface interfaces to obtain images of impedance contrasts within subsurface geologic structures. Seismic reflection data often contain no primary reflection waves from steeply-dipping fault zones, and multiple reflections from these fault zones are much weaker than primary reflections from stratigraphic layers. Therefore, it is a great challenge to directly image steeply-dipping fault zones.

The primary objective of the Phase I research of this project was to address the challenge of directly imaging steeply-dipping fault zones using seismic reflection data. During Phase I, we developed an novel elastic-wave reverse-time migration technique capable of directly imaging steeply-dipping fault zones. We implemented our new imaging method for the two-dimensional (2D) case, and validated its capability of imaging steeply-dipping fault zones using synthetic seismic-reflection data.

The objective of the Phase II research of this project was to study the field data applicability of our new imaging algorithms. We developed a 3D elastic reverse-time migration imaging algorithm, applied our 3D imaging algorithm to the seismic data acquired at Soda Lake geothermal field, refined the velocity model using full-waveform inversion, and conducted migration imaging using the new velocity model to further improve the images of fault zones at the Soda Lake geothermal field.

4 Phase I to Phase II

The success criteria of the Phase I research of this project were

1. ***Develop algorithm for 2D angle-domain imaging condition***: We developed a novel 2D elastic reverse-time migration (ERTM) imaging technique with a wavefield-separation imaging condition and an angle-domain imaging condition.

2. ***Validate 2D imaging capability of detecting fault zones using 2D synthetic data***: We validated the 2D imaging capability of our ERTM method for detecting steeply-dipping fault zones using synthetic elastic data for a model containing a steeply-dipping fault zones and a preliminary 2D geophysical model from the Soda Lake geothermal field containing several steeply-dipping fault zones.

Reverse-time migration solves full scalar-wave equation in heterogeneous media and is a powerful tool for high-resolution subsurface imaging using single-component or pressure data (Baysal et al., 1983; McMechan, 1983; Whitmore, 1983; Liu et al., 2011). It uses single-component seis-

mic data for migration imaging. We have recently applied reverse-time migration with a wavefield-separation imaging condition to imaging fault zones, and revealed some fault zones that are unknown before using single-component seismic data acquired at Jemez Pueblo in New Mexico (Huang and Albrecht, 2011; Huang et al., 2011).

Elastic reverse-time migration (ERTM) is based on solving the elastic-wave equation in complex media for forward propagation of wavefields from sources and backward propagation of recorded seismic reflection data from receivers (Chang and McMechan, 1987). ERTM can handle all the complex waveforms and has no dip limitation. It has been shown as the most promising tool for high-resolution images of complex subsurface structures. However, conventional ERTM imaging conditions face some difficulties (Yoon et al., 2004). One of them is the low-wavenumber artifacts in migration images. This is caused by the cross correlation of full waves of source and receiver wavefields, which not only produces images at the reflectors, but also at other locations along the entire wave path. The other difficulty is related to multicomponent seismic data. During elastic-wave propagation, compressional (P) waves can be converted to shear (S) waves, and S waves can be converted to P waves at interfaces. For converted waves, the conventional imaging condition is no longer valid, leading to poor images. This is due to the polarization of converted waves. Destructive interference occurs when stacking PS or SP images with mixed signs of the polarization. Different approaches have been developed to address this issue (e.g., Mulder and Plessix, 2004; Kaelin and Guitton, 2006; Denli and Huang, 2008; Yan and Xie, 2010; Du et al., 2012).

We recently developed a wavefield separation imaging condition for elastic reverse-time migration in the time domain (Denli and Huang, 2008). This imaging condition can reduce the low-wavenumber image artifact of elastic reverse-time migration like that for reverse-time migration using pressure waves or single-component data (Liu et al, 2011). The wavefield separation method was recently used in elastic reverse-time migration in the frequency domain (Chung et al., 2012). However, it is straightforward to extend the two-dimensional (2D) elastic-wave reverse-time migration method in the time domain to the three-dimensional (3D) case, while it is difficult to implement 3D elastic reverse-time migration in the frequency domain. Therefore, we focus on the time-domain elastic reverse-time migration.

In the Phase I of this project, we have developed a novel 2D ERTM imaging technique to reduce these artifacts and directly image steeply-dipping fault zones using surface seismic reflection data. We employ our elastic wavefield separation scheme (Denli and Huang, 2008) to obtain downgoing and upgoing waves, and leftgoing and rightgoing waves of P- and S-waves within an imaging region. Imaging with these wavefields eliminates the low-wavenumber image noise caused by cross-correlation of full wavefields. We then exploit an imaging condition in the angle domain to properly account for the S-wave polarization. Therefore, ERTM produces compressional-to-compressional (PP), compressional-to-shear (PS), shear-to-compressional (SP), and shear-to-shear (SS) images.

We have first validated our ERTM imaging technique using synthetic elastic-wave reflection data for a stratigraphic layered model containing a 75°-dip fault zone. Our efforts are primarily focused on the capability of our ERTM for imaging steeply-dipping fault zones. We have then applied our new ERTM technique to image several steeply-dipping fault zones in a geophysical model built using geologic features found at the Soda Lake geothermal field, and obtained signifi-

cantly improved images of the fault zones compared to those obtained using conventional ERTM. We have observed that seismic data from explosive sources yield best PP and PS images of fault zones, and seismic data acquired using vertical and horizontal sources produce best SP and SS images of fault zones.

DOE GTO approved to proceed to Phase II of the project in February, 2013. In Phase II of this project, we have developed our imaging algorithm for three-dimensional (3D) imaging, and applied the imaging technique to the field seismic-reflection data acquired at the Soda Lake geothermal field.

5 Summary of Accomplishments

During the course of the project, we conducted the following research topics to fulfill the primary project goal of imaging fracture/fault zones:

1. Developed novel finite-difference modeling methods that are used both in full-waveform inversion and reverse-time migration;
2. Developed a novel method method to reduce computer memory requirement for wavefield backpropagation, a key step in both reverse-time migration and full-waveform inversion;
3. Developed novel full-waveform inversion methods using acoustic- (single component) and elastic-wavefields (multiple components)) to obtain improved velocity models needed for accurate reverse-time migration;
4. Developed novel imaging conditions for reverse-time migration;
5. Developed novel reverse-time migration methods to improve migration images; and
6. Applied 3D full-waveform inversion and 3D reverse-time migration to the 3D surface seismic data acquired at the Soda Lake geothermal field.

The relationship among these research topics are shown in Fig. 1.

In the following, we describe our accomplishments under each task in detail.

5.1 Develop a novel 2D elastic reverse-time migration imaging technique and validate the algorithm using synthetic data for a 2D velocity model

Our 2D and 3D reverse-time migration imaging and full-waveform inversion are based on solving the wave equation using a finite difference method. We have developed a novel finite-difference modeling to improve the modeling efficiency and accuracy and new reverse-time migration methods.

We developed an efficient finite-difference method with high-order accuracy in both time and space domains for modelling scalar-wave propagation. For modelling large-scale 3-D scalar-wave propagation, the finite-difference (FD) method with high-order accuracy in space but second-order accuracy in time is widely used because of its relatively low requirements of computer memory.We develop a novel staggered-grid (SG) FD method with high-order accuracy not only in space, but also in time, for solving 2- and 3-D scalar-wave equations. We developed a new method to de-

termine the coefficients of the FD operator in the joint time-space domain to achieve high-order accuracy in time while preserving high-order accuracy in space. Our new FD scheme is based on a stencil that contains a few more grid points than the standard stencil. It is $2M^{th}$-order (M=1, 2, ...) accurate in space and fourth-order accurate in time when using 2M grid points along each axis and wavefields at one time step as the standard SGFD method. We validated the accuracy and efficiency of our new FD scheme using dispersion analysis and numerical modelling of scalar-wave propagation in 2- and 3-D complex models with a wide range of velocity contrasts. For media with a velocity contrast up to five, our new FD scheme is approximately two times more computationally efficient than the standard SGFD scheme with almost the same computer-memory requirement as the latter. Our numerical experiments demonstrated that our new FD scheme loses its advantages over the standard SGFD scheme if the velocity contrast is 10. However, for most large-scale geophysical applications, the velocity contrasts often range approximately from 1 to 3. Our new method is thus particularly useful for large-scale 3-D scalar-wave modelling for full-waveform inversion and reverse-time migration. Our journal paper (Tan and Huang, 2014, Geophys. J. Int. 197, 1250-1267) in the appendix describes our new modeling method.

We developed a staggered-grid finite-difference scheme optimized in the time-space domain for modeling scalar-wave propagation in geophysical problems. For modeling scalar-wave propagation in geophysical problems using finite-difference schemes, optimizing the coefficients of the finite-difference operators can reduce numerical dispersion. Most optimized finite-difference schemes for modeling seismic-wave propagation suppress only spatial but not temporal dispersion errors. We developed a novel optimized finite-difference scheme for numerical scalar-wave modeling to control dispersion errors not only in space but also in time. Our optimized scheme is based on a new stencil that contains a few more grid points than the standard stencil. We designed an objective function for minimizing relative errors of phase velocities of waves propagating in all directions within a given range of wavenumbers. Dispersion analysis and numerical examples demonstrate that our optimized finite-difference scheme is computationally up to 2.5 times faster than the optimized schemes using the standard stencil to achieve the similar modeling accuracy for a given 2D or 3D problem. Compared with the high-order finite-difference scheme using the same new stencil, our optimized scheme reduces 50 percent of the computational cost to achieve the similar modeling accuracy. This new optimized finite-difference scheme is particularly useful for large-scale 3D scalar-wave modeling, full-waveform inversion and reverse-time migration. Our journal paper (Tan and Huang, 2014, Journal of Computational Physics 276, 613-634) in the appendix describes the new method.

We developed a new method for reducing the computer memory requirement for 3D reverse-time migration with a boundary-wavefield extrapolation method. Reverse-time migration (RTM) using the cross-correlation imaging condition and full-waveform inversion require that the forward-propagated source wavefield and the backward-propagated receiver wavefield be accessible within the imaging/inversion domain at the same time step. There are two categories of methods to balance the computer memory requirement and the computational complexity of RTM: checkpointing methods and source-wavefield reconstruction methods. We developed a new source-wavefield reconstruction method to improve the balance between the computer memory requirement and the computational complexity of RTM. During the forward simulation of the source wavefield, we stored boundary wavefields only at one or two layers of spatial grid points and reconstructed the back-propagated source wavefield at the same time step as that of the back-propagated re-

ceiver wavefield, using a high-order wave-equation extrapolation scheme. One conventional RTM method uses boundary wavefields stored at multiple layers of spatial grid points and a high-order finite-difference (FD) scheme to reconstruct the backpropagated source wavefield. For an FD scheme with the eighth or sixteenth order of accuracy in space, our new method used only 37.5% of the computer memory required by this conventional method to store the boundary wavefields. This reduction of computer memory usage is significant because storing the boundary wavefields consumes most of the computer memory required for 3D migration using reconstructed source wavefields. Moreover, our method maintained the spatial order of accuracy of the FD scheme for the entire imaging domain, whereas some conventional methods reduce the spatial-order accuracy of the FD scheme near the boundaries to back-propagate the source wavefield to decrease the computer memory requirement. We validated our method using synthetic seismic data. Our method produced 2D and 3D migration images of complex subsurface structures as accurate as those yielded using an RTM method without reducing the spatial order of accuracy near the boundaries. Our journal paper (Tan and Huang, 2014, GEOPHYSICS 79, S185-S194) in the appendix gives the detailed description of the method.

We developed novel acoustic- and elastic-waveform inversion using a modified total-variation regularization scheme. Subsurface velocities within the Earth often contain piecewise-constant structures with sharp interfaces. Acoustic- and elastic-waveform inversion (AEWI) usually produces smoothed inversion results of subsurface geophysical properties. We developed novel AEWI methods using a modified total-variation regularization scheme to preserve sharp interfaces in piecewise constant structures and improve the accuracy of compressional- and shear-wave velocity inversion. We used an alternating-minimization algorithm to solve the minimization problem of our new waveform inversion methods. We decoupled the original optimization problem into two simple subproblems: a standard waveform inversion subproblem with the Tikhonov regularization and a standard L_2-TV subproblem. We solved these two subproblems separately using the non-linear conjugate-gradient and split-Bregman iterative methods. The computational costs of our new waveform inversion methods using the modified total-variation regularization scheme are comparable to those of conventional waveform inversion approaches. Our numerical examples using synthetic seismic reflection data showed that our new methods not only preserve sharp interfaces of subsurface structures, but also significantly improve the accuracy of compressional- and shear-wave velocity inversion.

Reverse-time migration has the potential to image complex subsurface structures, including steeply-dipping fault zones, but the method requires an accurate velocity model. Acoustic- and elastic-waveform inversion is a promising tool for high-resolution velocity model building. Because of the ill-posedness of acoustic- and elastic-waveform inversion, it is a great challenge to obtain accurate velocity models containing sharp interfaces. To improve velocity model building, we develop an acoustic- and elastic-waveform inversion method with an interface-guided modified total-variation regularization scheme to improve the inversion accuracy and robustness, particularly for models with sharp interfaces and steeply-dipping fault zones with widths much smaller than the seismic wavelength. The new regularization scheme incorporates interface information into seismic full-waveform inversion. The interface information of subsurface interfaces is obtained iteratively using migration imaging during waveform inversion. Seismic migration is robust for subsurface imaging. Our new acoustic- and elastic-waveform inversion takes advantage of the robustness of migration imaging to improve velocity estimation. We use synthetic seismic data

for a complex model containing sharp interfaces and several steeply-dipping fault zones to validate the improved capability of our new acoustic- and elastic-waveform inversion method. Our inversion results are much better than those produced without using interface-guided regularization. Acoustic- and elastic-waveform inversion with an interface-guided modified total-variation regularization scheme has the potential to accurately build subsurface velocity models with sharp interfaces and/or steep fault zones.

The details of the aforementioned inversion methods can be found in the our publications and a journal manuscript in the appendix (Lin and Huang, 2015, Geophys. J. Int. 200, 489-502; Lin and Huang, Proceedings of 39th Stanford Geothermal Workshop; Lin and Huang, 2017, Pure and Applied Geophysics, under review).

We developed a new least-squares reverse-time migration with a wavefield-separation imaging condition and updated source wavefields. Directly imaging steeply dipping fault zones is difficult for conventional migration, including reverse-time migration (RTM). We developed a new least-squares RTM (LSRTM) method to directly image steeply dipping fault zones. The method uses a wavefield-separation imaging condition and updated source wavefields during each iteration. Our new imaging method produces horizontal-looking images that show mostly steeply dipping fault zones. Conventional least-squares RTM does not update source wavefields and cannot directly image vertical fault zones. We numerically determined that it is crucial to update source wavefields to image steeply dipping fault zones. Using synthetic seismic data, we proved that our new LSRTM method can directly image steeply dipping fault zones with dipping angles up to 90. Compared with conventional LSRTM, our LSRTM method was less sensitive to the smoothness and the velocity error of the initial migration velocity model. Our journal paper (Tan and Huang, 2014, GEOPHYSICS 79, S195-S205) in the appendix describes our new method.

We developed a new least-squares reverse-time migration with modified total-variation regularization. Least-squares reverse-time migration images may contain significant artifacts when data are too sparse. We developed a new least-squares reverse-time migration method with a modified total-variation regularization scheme to improve the image quality and reduce image artifacts. The modified total-variation regularization is a hybrid regularization scheme, taking advantages of the Tikhonov regularization and the total-variation regularization. To improve the convergence and robustness of our new method, we decoupled the original optimization problem into two simple subproblems: a least-squares reverse-time migration subproblem with the Tikhonov regularization and a L2-total-variation denoising subproblem. We solved these two subproblems separately using the preconditioned conjugate-gradient and split Bregman iterative methods. We validated the improved imaging capability of our new method using synthetic surface seismic data for a 2D geophysical model constructed using geologic features found at the Soda Lake geothermal site. Our numerical examples demonstrated that the new method significantly improves the image quality and reduce image artifacts for noise-free and noisy data compared with those obtained using conventional least-squares reveres-time migration. We presented the method in a peer-reviewed proceedings paper in appendix (Lin and Huang, 2015, Expanded Abstracts of 2015 SEG Annual Meeting).

We developed two new imaging conditions for reverse-time migration. Elastic reverse-time migration needs to properly handle the shear-wave polarization during imaging using compressional-to-shear or shear-to-compressional converted waves. Polarity distribution analysis of Poynting

vectors is a computationally efficient method for polarization corrections. A limitation of the Poynting vector imaging condition is that it assumes only one dominant direction of wave propagation at each spatial point for any given time and thus is not very accurate in complex regions with complicated wavefields. We developed a computationally efficient imaging condition for elastic reverse-time migration to directly image steeply-dipping fault zones. We first separated the forward-propagating source wavefield and the backward-propagating receiver wavefield into left- and right-going, or down-going and up-going waves, and then apply the Poynting-vector imaging condition to the separated wavefields. After wavefield separation, the inaccuracy of the Poynting-vector imaging condition in complex regions is alleviated. We built a geophysical model using geologic features found at the Soda Lake geothermal field and generate synthetic multi-component seismic reflection data. The model contains several steeply-dipping fault zones. We validated the improved imaging capability of our new imaging condition for elastic reverse-time migration using the synthetic data. Our numerical results demonstrated that our new elastic reverse-time migration with the combined wavefield-separation and Poynting-vector imaging condition produces high-resolution images of steeply-dipping fault zones, while its computational cost is approximately one order of magnitude lower than that with the space-lag imaging condition for the 2D case.

The conventional cross-correlation imaging condition for elastic reverse-time migration (ERTM) produces significant artifacts. We developed an excitation amplitude imaging condition for ERTM to remove migration artifacts. During the forward propagation of the source wavefield, we stored the maximum amplitude of the wavefield and the corresponding excitation time for each imaging point, and apply the cross-correlation imaging condition only at the excitation time and when the amplitude of the receiver wavefield at this excitation time satisfies a certain criterion. We demonstrated using synthetic multicomponent seismic data that our excitation amplitude imaging condition effectively removes migration artifacts for both PP and PS images. Our new imaging condition also significantly improves the computational efficiency and reduces the computer-memory requirement for ERTM.

The aforementioned two new imaging conditions are described in two conference proceedings papers in the appendix (Chen and Huang, 2014, Proceedings of 39th Stanford Geothermal Workshop; Chen and Huang, 2014, Expanded Abstracts of 2014 SEG Annual Meeting).

We developed a novel 2D elastic reverse-time migration imaging technique with a wavefield-separation imaging condition and an angle-domain imaging condition for directly imaging steeply-dipping fault zones in geothermal fields with multicomponent seismic data. We have tested the method using 2D synthetic data for a Soda Lake velocity model.

For characterizing geothermal systems, it is important to have clear images of steeply-dipping fault zones because they may confine the boundaries of geothermal reservoirs and influence hydrothermal flow. Elastic reverse-time migration (ERTM) is the most promising tool for subsurface imaging with multicomponent seismic data. However, conventional ERTM usually generates significant artifacts caused bythe cross correlation of undesired wavefields and the polarity reversal of shear waves. In addition, it is difficult for conventional ERTM to directly image steeply-dipping fault zones. We developed a new ERTM imaging method reduce these artifacts and directly image steeply-dipping fault zones. In our new ERTM method, forward-propagated source wavefields and backward-propagated receiver wavefields are decomposed into compressional (P) and shear (S) components. Each component of these wavefields is separated into left- and right-going, or down-

going and upgoing waves. The cross correlation imaging condition is applied to the separated wavefields along opposite propagation directions. For converted waves (P-to-S or S-to-P), the polarity correction is applied to the separated wavefields basedon the analysis of Poynting vectors. Numerical imaging examples of synthetic seismic data demonstrated that our new ERTM method produces high-resolution images of steeply-dipping fault zones.

Elastic reverse-time migration (ERTM) has great advantages over other techniques in imaging steep fault zones and complex structures. ERTM imaging requires an accurate velocity model, and elastic-waveform inversion is a promising tool for improving subsurface velocity models. We studied how the imaging of fault zones would be improved when combing ERTM with elastic-waveform inversion. We used elastic-waveform inversion to update a velocity model containing several steep fault zones, and employ ETRM to image the faults. We demonstrated using synthetic seismic data for a fault model of the Soda Lake geothermal field that the images of fault zones are greatly improved with the combination of ERTM and elastic-waveform inversion.

Our new methods and numerical examples are presented in four papers in appendix (Chen and Huang, 2013, GRC Transactions 37, 999-1003; Chen and Huang, 2013, Proceedings of 38th Stanford Geothermal Workshop; Tan and Huang, 2014, Proceedings of 39th Stanford Geothermal Workshop; Chen and Huang, 2015, Geothermics 57, 238-245.).

We tested the 2D elastic reverse-time migration imaging technique using field data in Section 5.2, implemented a 3D RTM imaging condition based on implicit directional wavefield separation in Section 5.3, adopted a waveform-correlation based objective functional in our 2D and 3D acoustic- and elastic-waveform inversion algorithms in Section 5.4, and applied 2D and 3D elastic full-waveform inversion and reverse-time migration imaging to seismic data from Soda Lake geothermal field. Our imaging results demonstrated that our novel full-waveform inversion and reverse-time migration unveil some zones that may be associated with steeply-dipping fault zones and/or fracture zones.

5.2 Test the 2D elastic reverse-time migration imaging technique using field data

The Soda Lake geothermal field is located in the south central part of the Carson Sink, about six miles northwest of the town of Fallon (Figure 5). It is surrounded by other operating geothermal fields such as Desert Peak, Bradys, Stillwater, and Salt Wells. The Soda Lake geothermal field contains several fault zones, as shown in a conceptual geological model in Fig. 6.

The 3D seismic surface data was acquired by Dawson Geo in June 2010 and processed by Geokinetics in August 2011. However, Magma Energy (U.S.) Corp. and Geokinetics did not keep a copy of processed, prestack seismic data. Vecta Oil and Gas Ltd. re-processed the data in 2015. The preprocessing steps include amplitude recovery, surface consistent amplitude scaling, elevation statics corrections, surface-consistent statics, time-variant spectral whitening, etc.

We extracted the source-receiver geometry from the processed data (Figure 7). Figure 8 shows a crossline slice of the initial velocity model built from migration velocity analysis.

We applied our elastic reverse-time migration (ERTM) to the 2D line data and the migration

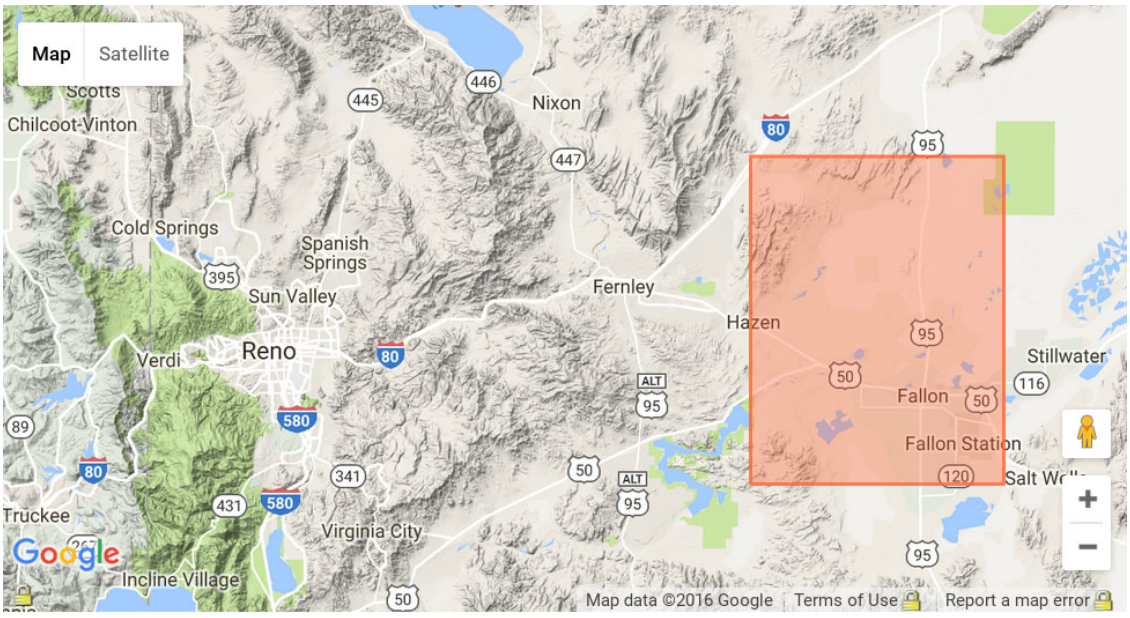

Figure 5: Map of the Soda Lake geothermal field location (the region denoted by the red rectangle).

velocity model for migration, and obtain the 2D PP and PS images shown in Figures 9 and 10, respectively.

5.3 Develop the 3D elastic reverse-time migration imaging technique

Conventional reverse-time migration (RTM) suffers from the problem of low-wavenumber image artifacts in migration image. Post-processing procedures can partially remove such noises, but can also alter the phase or other fundamental characteristics of migration images. Imaging condition based on explicit wavefield separation, i.e., Poynting vector wavefield separation, may not be accurate in complex subsurface structures. Meanwhile, Fourier-transform-based wavefield-separation imaging conditions are extremely expensive for 3D tasks.

We implemented a 3D RTM imaging condition based on implicit directional wavefield separation. For example, we can obtain the down-going RTM images using

$$I_{PP,d}(\mathbf{x}) = \sum_{N_s,N_r} \int_0^T \left[P_s P_r - \mathcal{H}_z(P_s)\mathcal{H}_z(P_r) - P_s\mathcal{H}_z(\mathcal{H}_t(P_r)) - \mathcal{H}_z(P_s)\mathcal{H}_t(P_r)\right] dt, \quad (1)$$

$$I_{PS,d}(\mathbf{x}) = \sum_{N_s,N_r} \int_0^T \left[P_s S_r - \mathcal{H}_z(P_s)\mathcal{H}_z(S_r) - P_s\mathcal{H}_z(\mathcal{H}_t(S_r)) - \mathcal{H}_z(P_s)\mathcal{H}_t(S_r)\right] dt, \quad (2)$$

where P and S represent the P- and S-wavefield, respectively, $\mathcal{H}_t$ is the Hilbert transform in time domain, and $\mathcal{H}_z$ is the Hilbert transform along z-direction, subscripts s and r represent the source and receiver wavefield, respectively. The spatial Hilbert transforms can be efficiently calculated with space-domain discrete convolution and therefore, computations of the imaging conditions in equations (1) and (2) can be much faster than Fourier-transform-based wavefield-separation imaging conditions for large 3D RTM imaging problems. The horizontal-looking images can be

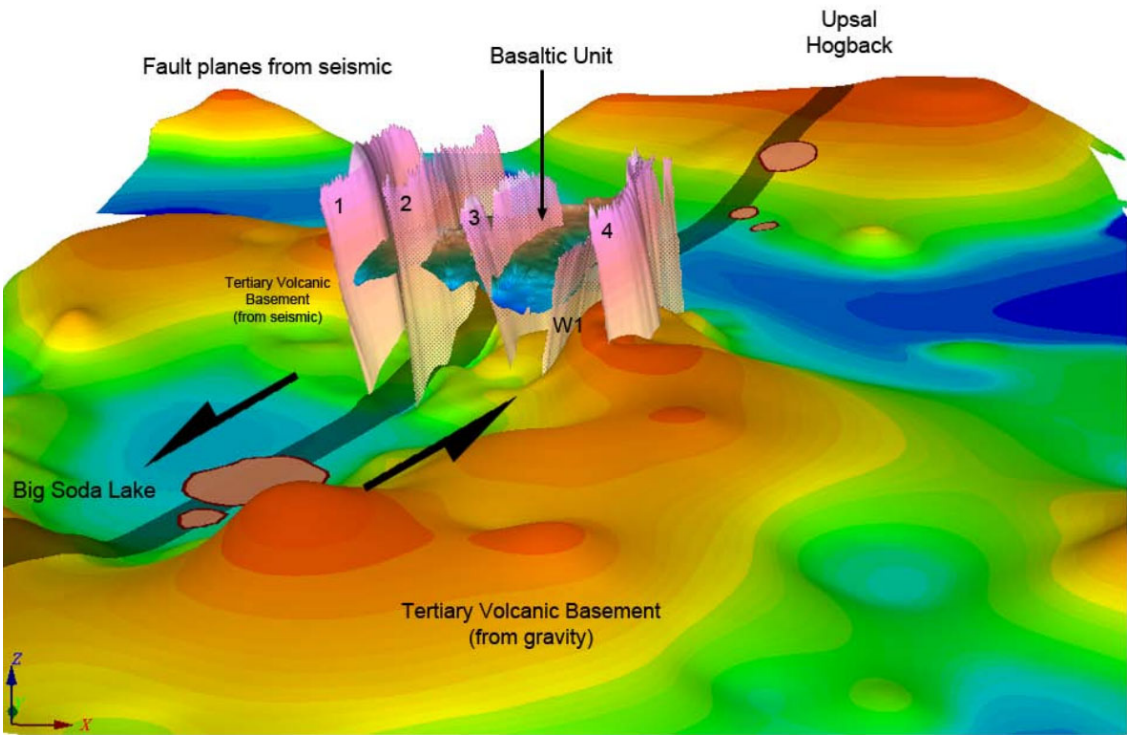

Figure 6: 3D oblique view of a conceptual geological model of the Soda Lake geothermal field (From Magma Energy Corp.).

obtained in a similar approach. These algorithms enable us to effectively and efficiently obtain clean migration images free from low-wavenumber image artifacts and those artifacts generated by large velocity gradients in a velocity model.

We developed a 3D elastic reverse-time migration algorithm using the above imaging conditions. The algorithm is implemented using Fortran and the Massage Passing Interface (MPI) parallel technique.

We conducted a series of numerical tests to validate both the effectiveness of our algorithm and the superiority of our method compared with the conventional ERTM.

5.4 Refine the prestack-depth-migration velocity model

The objective is to refine the prestack depth migration velocity model using full-waveform inversion.

Conventional full-waveform inversion (FWI) usually assume L_2-norm objective functional:

$$\chi(\mathbf{m}) = \frac{1}{2}||\mathbf{d}_0 - \mathbf{d}(\mathbf{m})||_2^2, \tag{3}$$

where $\mathbf{m}$ is the model, $\mathbf{d}_0$ is the observed data, and $\mathbf{d}(\mathbf{m})$ is the synthetic data. This objective functional can suffer from serious amplitude mismatch problem for field data full-waveform inversion, because it is usually difficult to accurately determine the wavelet signature for every possible shot

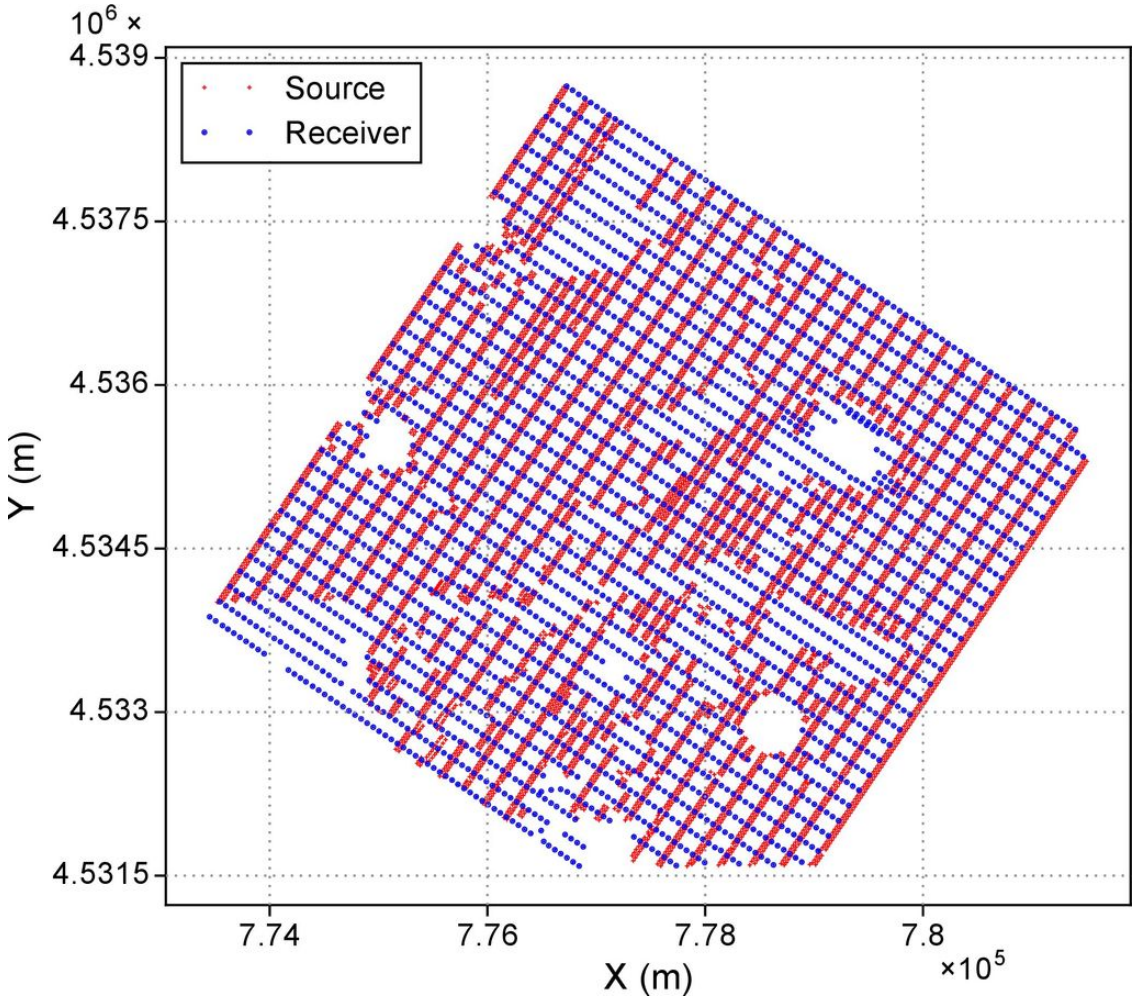

Figure 7: Source-receiver geometry of the Soda Lake 3D surface seismic data.

gather, amplitudes of processed seismic data are usually not preserved during data processing, and seismic-wave attenuation.

We therefore adopted a waveform-correlation based objective functional in our 2D and 3D acoustic- and elastic-waveform inversion algorithms:

$$\chi(\mathbf{m}) = \sum_{N_s,N_r} \int_0^T \left[1 - \frac{\mathbf{d}_0\mathbf{d}(\mathbf{m})}{||\mathbf{d}_0||_2||\mathbf{d}(\mathbf{m})||_2}\right] dt, \tag{4}$$

where

$$||\mathbf{d}_0||_2 = \left(\int_0^T \mathbf{d}_0^2 dt\right)^{1/2}, \qquad ||\mathbf{d}(\mathbf{m})||_2 = \left(\int_0^T \mathbf{d}(\mathbf{m})^2 dt\right)^{1/2}. \tag{5}$$

The objective functional in equation (4) can bypass the amplitude matching criterion of the conventional objective functional in equation (3), while can still maximize the zero time lag cross-correlation between the field and synthetic data. When the field data and synthetic data differ only by a scale factor in amplitude, the correlative objective functional can correctly gives zero misfit. It is therefore more robust in field data applications.

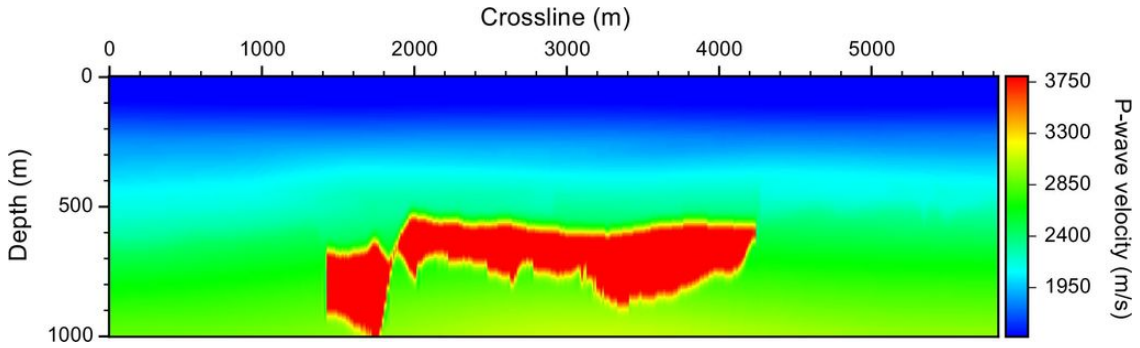

Figure 8: Initial 2D velocity model obtained from migration velocity analysis.

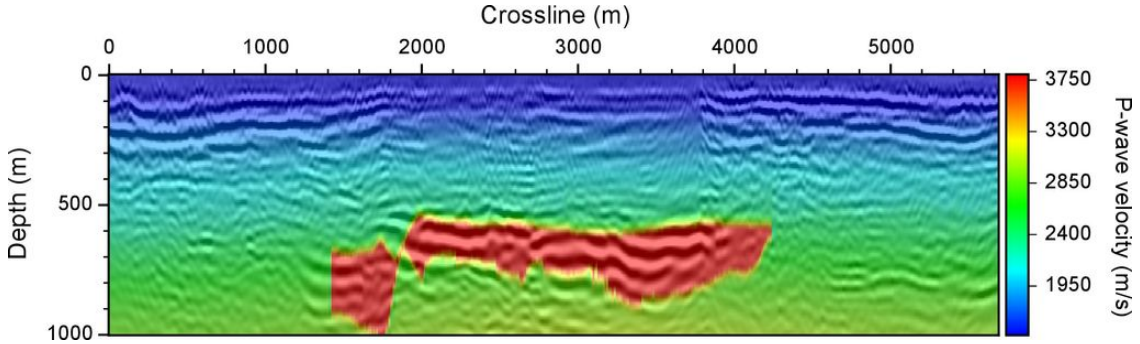

Figure 9: 2D elastic reverse-time migration PP image obtained with the initial velocity model.

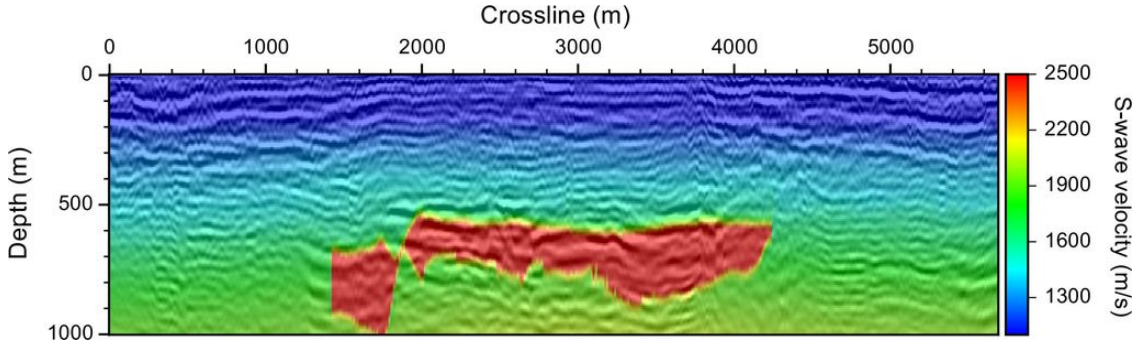

Figure 10: 2D elastic reverse-time migration PS image obtained with the initial velocity model.

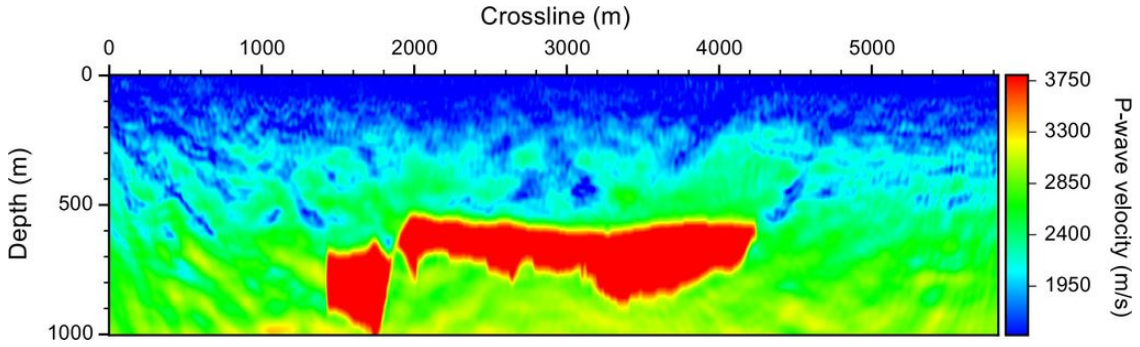

Figure 11: A 2D velocity model of Soda Lake geothermal field obtained using LANL's full-waveform inversion algorithm.

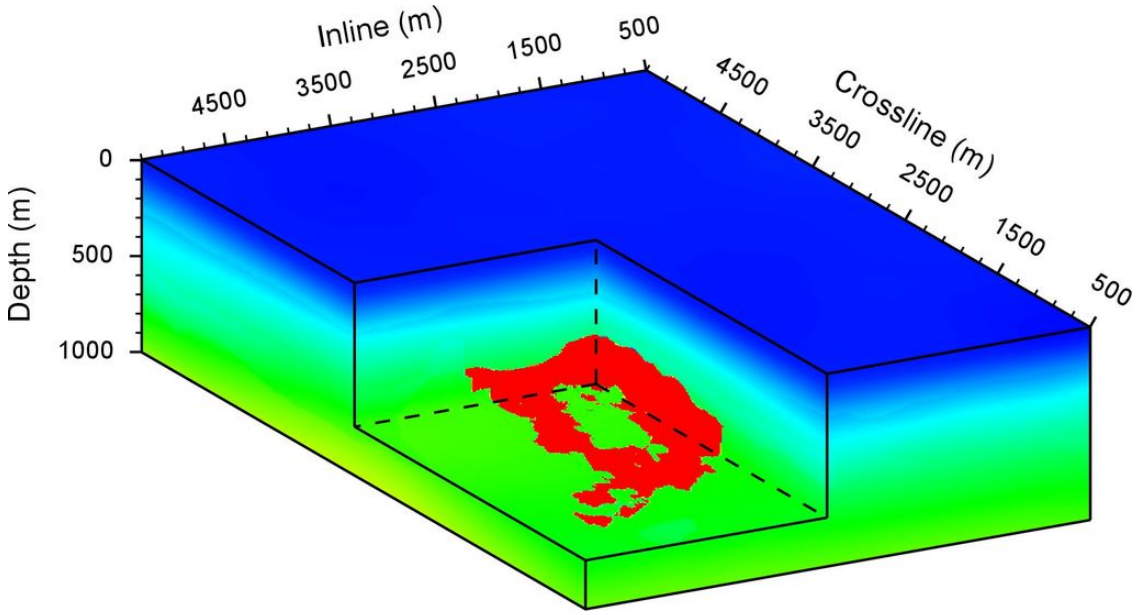

Figure 12: 3D initial velocity model built using migration velocity analysis with view angle 3.

We applied our new full-waveform inversion to 2D and 3D Soda Lake seismic data to obtain high-resolution velocity models.

Figure 8 shows the velocity model built using migration velocity analysis. We used this model as the initial model for our 2D full-waveform inversion. We obtained a high-resolution velocity model in 11 using a multiscale, wavefield-energy-preconditioned full-waveform inversion strategy based on the waveform-correlation objective functional.

Figure 12 shows the initial velocity model built using migration velocity analysis. We used this 3D velocity model as the initial model, and apply our 3D full-waveform inversion algorithm to 3D seismic data from Soda Lake geothermal field. Again, we employ a multiscale, wavefield-energy-preconditioned full-waveform inversion strategy based on the waveform-correlation objective functional. The resulting high-resolution 3D velocity model is shown in Figure 13.

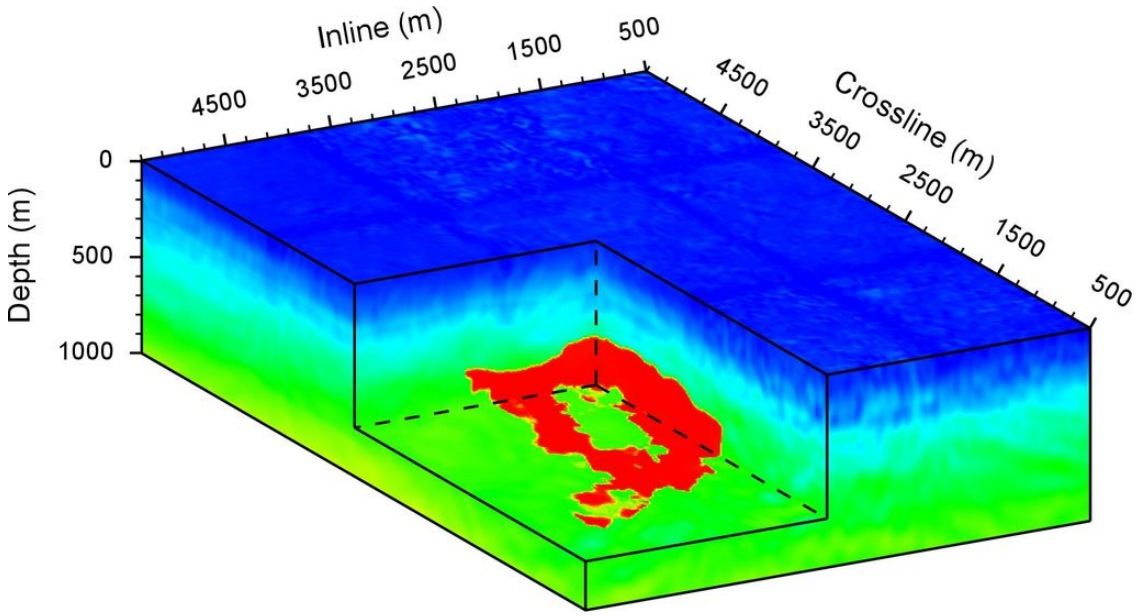

Figure 13: 3D inverted velocity model built using multiscale correlative elastic-waveform inversion with view angle 3.

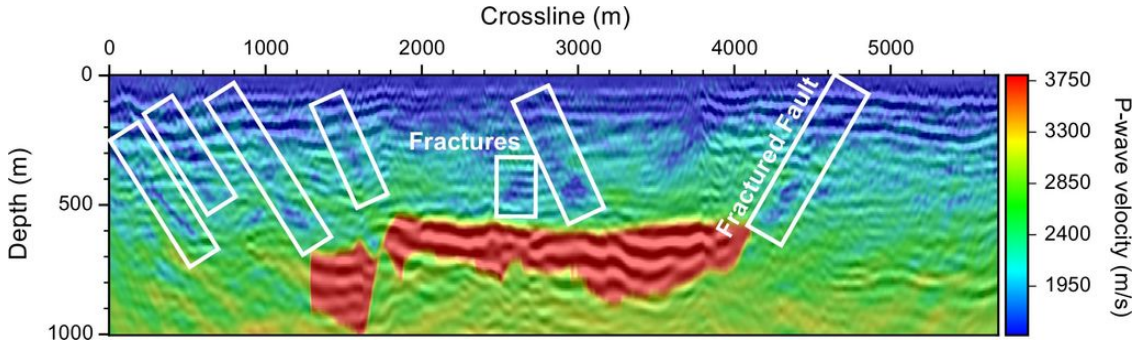

Figure 14: 2D elastic reverse-time migration PP image obtained with the FWI velocity model.

5.5 Apply 2D and 3D elastic reverse-time migration imaging to seismic data from Soda Lake geothermal field

We applied the 2D elastic reverse-time migration imaging based on wavefield separation to the 2D data from Soda Lake geothermal field using the improved velocity model obtained from our full-waveform inversion. The new 2D PP and PS images are shown in Figures 14 and 15, respectively. The low-velocity zones may be associated with faults/fracture zones.

We then applied our 3D elastic reverse-time migration imaging technique to the 3D seismic data from Soda Lake geothermal field using the original prestack-depth-migration velocity model. Figures 16 show the 3D PP image obtained using our ERTM with a wavefield-separation imaging condition and initial velocity models from migration velocity analysis.

Figure 17 shows the 3D PS image obtained with our ERTM with the wavefield-separation imaging condition and the initial velocity models from migration velocity analysis.

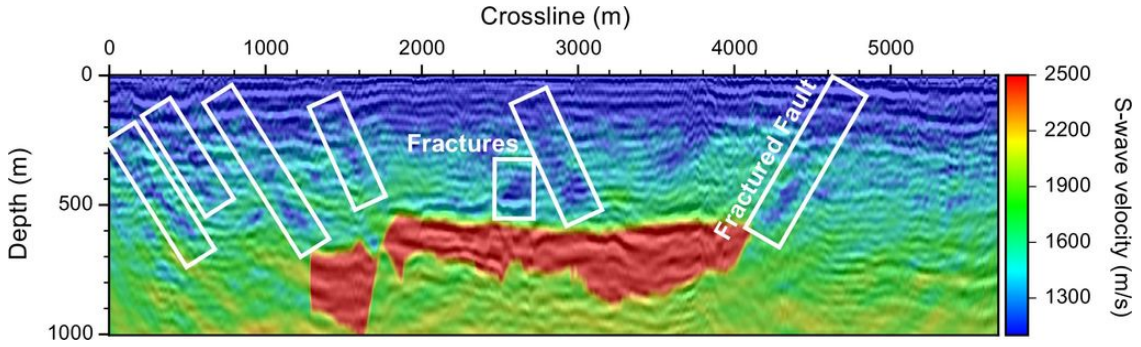

Figure 15: 2D elastic reverse-time migration PS image obtained with the FWI velocity model.

Figure 18 shows the 3D PP image obtained using our ERTM with a wavefield-separation imaging condition and the inverted velocity models built from our elastic-waveform inversion.

Figure 19 shows the 3D PS image produced using our ERTM with a wavefield-separation imaging condition the inverted velocity models built from our elastic-waveform inversion.

6 List of Publications

The following papers resulted from this project research.

Chen, T. and Huang, L., 2013. Directly imaging steep fault zones using multicomponent seismic data, Proceedings of Thirty-Eighth Workshop on Geothermal Reservoir Engineering, Stanford University, Stanford, California, February 11-13, 2013, SGP-TR-198, 1193-1200.

Chen, T. and Huang, L., 2013. Imaging Faults Using Elastic Reverse-Time Migration With Updated Velocities of Waveform Inversion, GRC Transactions, 37, 999-1003.

Chen, T. and Huang, L., 2014. Elastic reverse-time migration with an excitation amplitude imaging condition, Expanded Abstracts, 2014 SEG Annual Meeting, 1868-1872.

Chen, T. and Huang, L., 2014. Imaging Steeply-Dipping Fault Zones Using Elastic Reverse-Time Migration with a Combined Wavefield-Separation and Poynting-Vector Imaging Condition, PROCEEDINGS, Thirty-Ninth Workshop on Geothermal Reservoir Engineering Stanford University, Stanford, California, February 24-26, 2014 SGP-TR-202, 1-12.

Lin, Y. and Huang, L., 2014. Building Subsurface Velocity Models with Sharp Interfaces and Steeply-Dipping Fault Zones Using Elastic-Waveform Inversion with Edge-Guided Regularization. PROCEEDINGS, Thirty-Ninth Workshop on Geothermal Reservoir Engineering Stanford University, Stanford, California, February 24-26, 2014 SGP-TR-202, 1-8.

Tan, S. and Huang, L., 2014. Reducing the computer memory requirement for 3D reverse-time migration with a boundary-wavefield extrapolation method. GEOPHYSICS, VOL. 79, NO. 5 (SEPTEMBER-OCTOBER 2014); P. S185-S194.

Tan, S. and Huang, L., 2014. Least-squares reverse-time migration with a wavefield-separation imaging condition and updated source wavefields. GEOPHYSICS, VOL. 79, NO. 5 (SEPTEMBER-OCTOBER 2014); P. S195-S205.

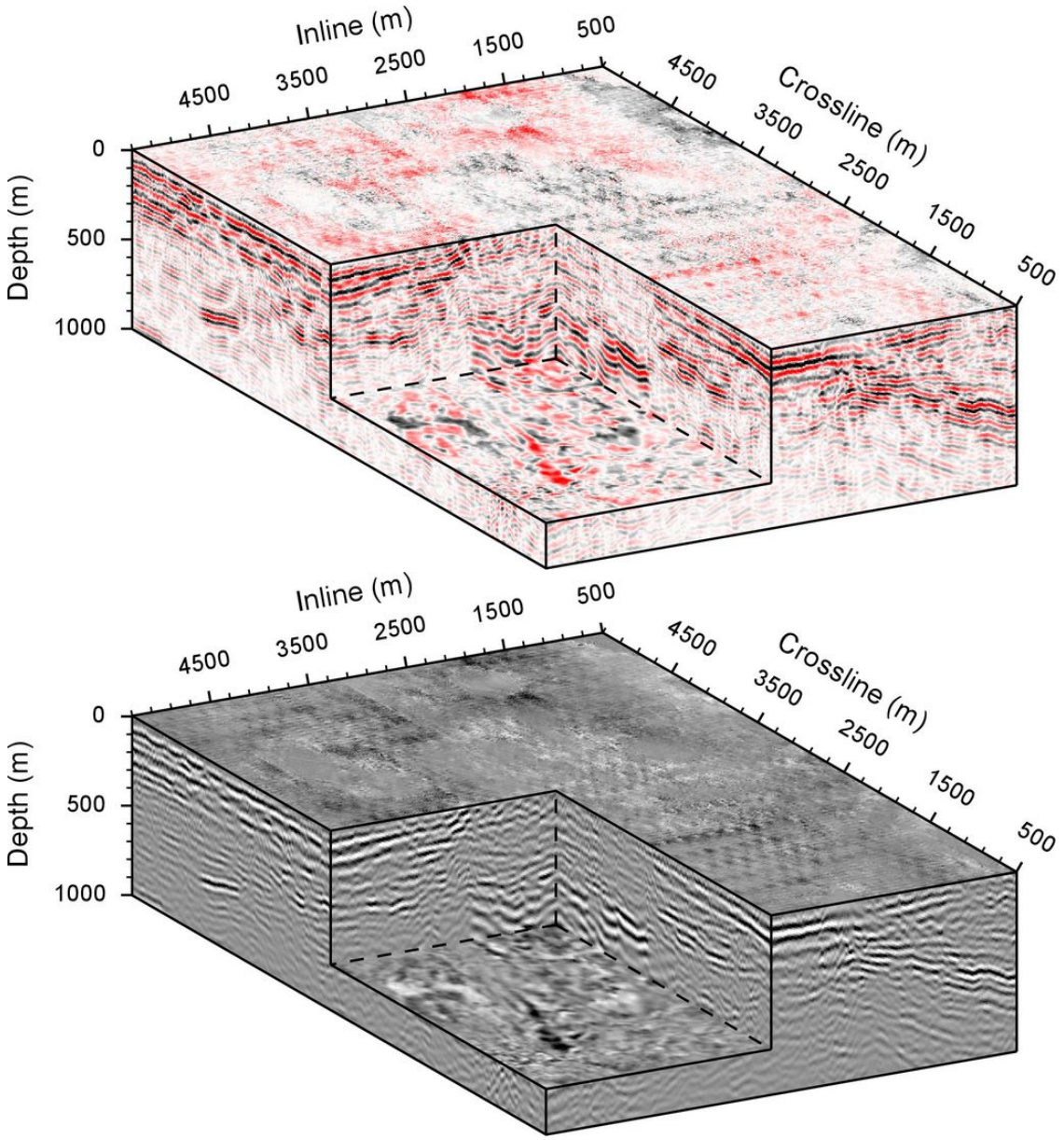

Figure 16: 3D elastic reverse-time migration PP image obtained with the original velocity model with view angle 3.

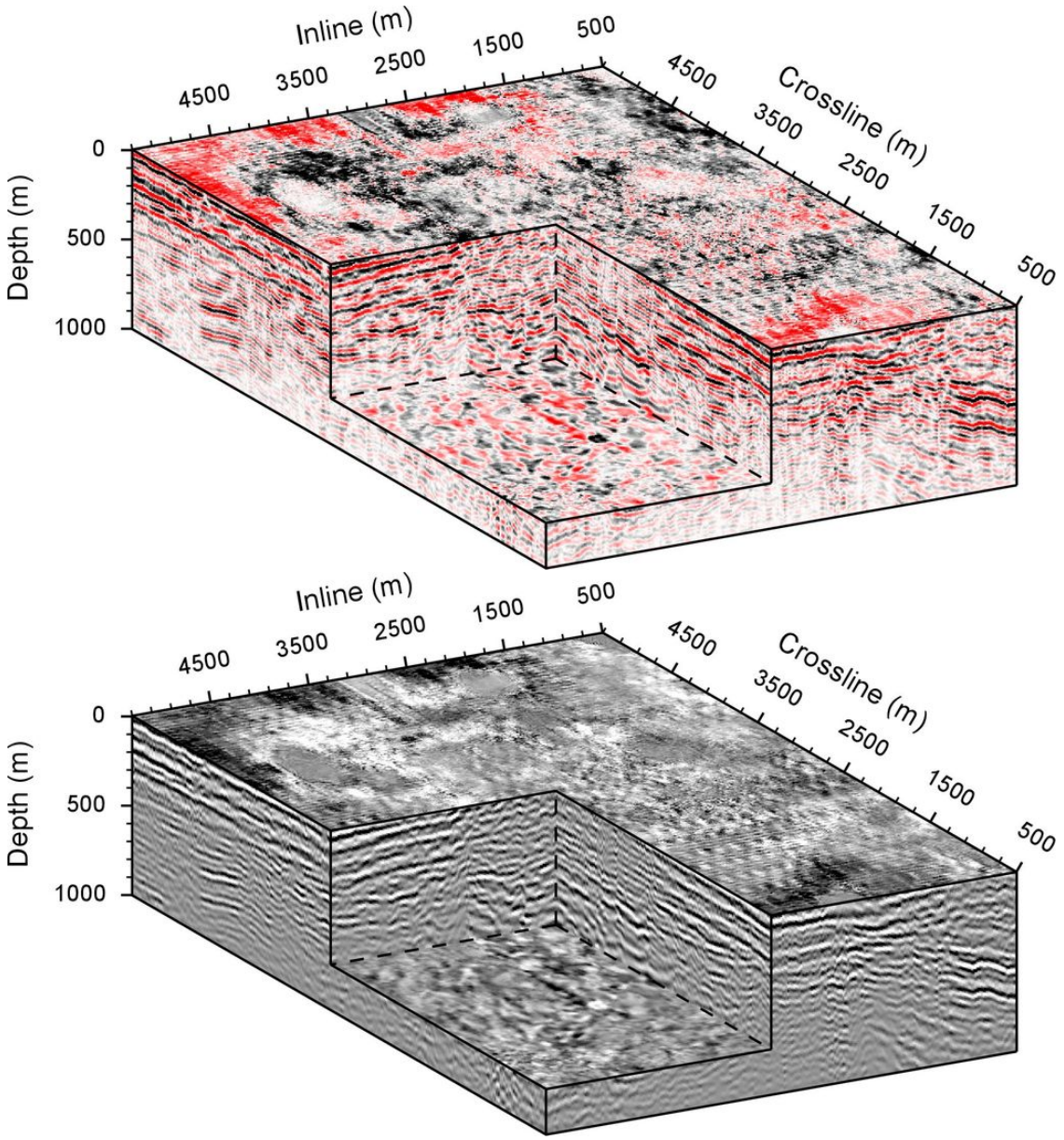

Figure 17: 3D elastic reverse-time migration PS image obtained with the original velocity model with view angle 3.

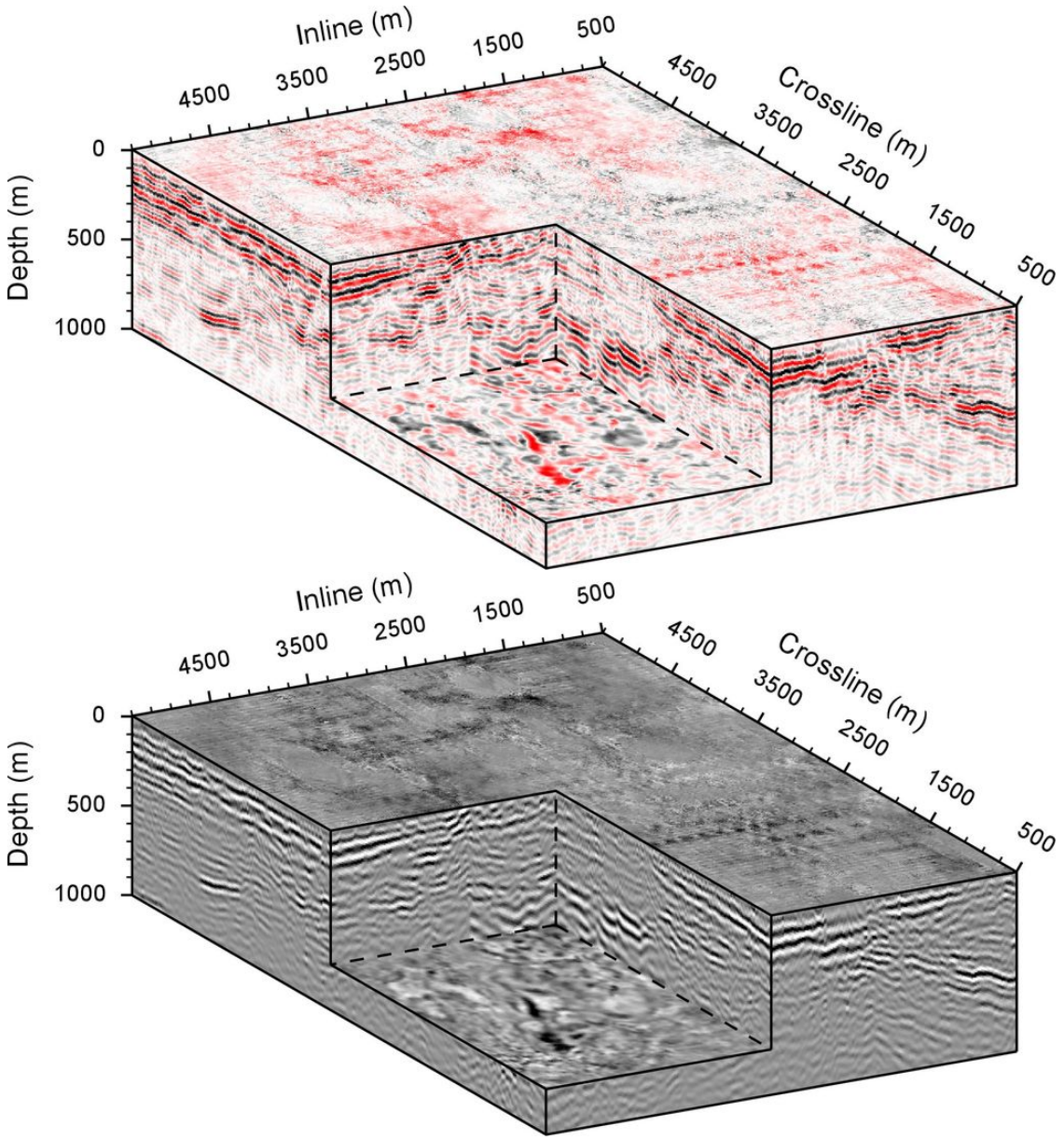

Figure 18: 3D elastic reverse-time migration PP image obtained with the inverted velocity model with view angle 3.

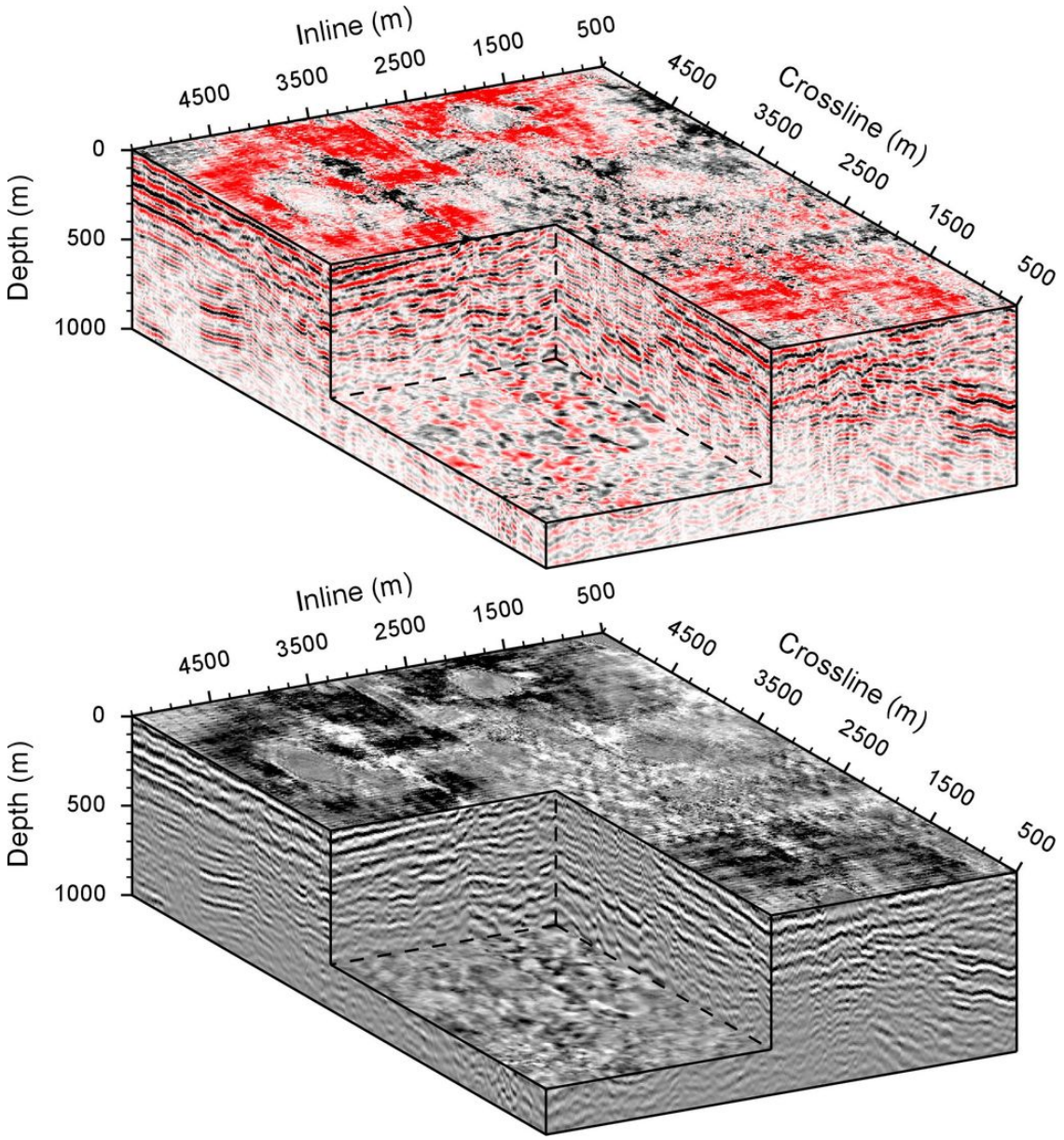

Figure 19: 3D elastic reverse-time migration PS image obtained with the inverted velocity model with view angle 3.

Tan, S. and Huang, L., 2014. An efficient finite-difference method with high-order accuracy in both time and space domains for modelling scalar-wave propagation. Geophys. J. Int. (2014) 197, 1250-1267.

Tan, S. and Huang, L., 2014. A staggered-grid finite-difference scheme optimized in the time-space domain for modeling scalar-wave propagation in geophysical problems. Journal of Computational Physics 276 (2014) 613-634.

Tan, S. and Huang, L., 2014. Imaging Steeply-Dipping Fault Zones Using a Novel Least-Squares Reverse-Time Migration Method. PROCEEDINGS, Thirty-Ninth Workshop on Geothermal Reservoir Engineering Stanford University, Stanford, California, February 24-26, 2014 SGP-TR-202, 1-6.

Chen, T. and Huang, L., 2015. Directly imaging steeply-dipping fault zones in geothermal fields with multicomponent seismic data, Geothermics 57 (2015) 238-245.

Lin, Y. and Huang, L., 2015. Least-squares reverse-time migration with modified total-variation regularization, Expanded Abstracts, 2015 SEG Annual Meeting, 4264-4269.

Lin, Y. and Huang, L., 2015. Acoustic- and elastic-waveform inversion using a modified total-variation regularization scheme. Geophys. J. Int. (2015) 200, 489-502.

Gao, K. and Huang, L., 2016. Building a High-Resolution Velocity Model with Full-Waveform Inversion: A Case Study for Soda Lake Geothermal Field, PROCEEDINGS, 41st Workshop on Geothermal Reservoir Engineering Stanford University, Stanford, California, February 22-24, 2016 SGP-TR-209, 1484-1488.

Gao, K. and Huang, L., 2017. High-Resolution Subsurface Imaging at Soda Lake Geothermal Field, PROCEEDINGS, 42nd Workshop on Geothermal Reservoir Engineering Stanford University, Stanford, California, February 13-15, 2017 SGP-TR-212, 1-6.

Lin, Y. and Huang, L., 2017. Building Subsurface Velocity Models with Sharp Interfaces Using Interface-Guided Seismic Full-Waveform Inversion. Pure and Applied Geophysics, under review.

7 Acknowledgements

This work was supported by the Geothermal Technologies Office (GTO) of the U.S. Department of Energy through contract DE-AC52-06NA25396 to Los Alamos National Laboratory. We thank strong support of GTO Program Managers Eric Hass, Mark Ziegenbein, Holly Thomas, and Brittany Segneri. We thank Holly Thomas for her careful review of this report and her valuable comments. We thank George Guthrie and David Coblentz of LANL for their help in preparing and reviewing this report. We thank Magma Energy (U.S.) Corp for providing us with raw seismic data acquired at the Soda Lake geothermal field. The computation was performed using supercomputers of LANL's Institutional Computing Program.

8 References

Baysal, E., D. D. Kosloff, and J. W. C. Sherwood, (1983), Reverse Time Migration, Geophysics, 48, 1514-1524.

Chang, W.-F. and McMechan, G. (1987), Elastic Reverse-Time Migration, Geophysics, 52, 1365-1375.

Chung, W., Sukjoon, P., Bae, H. S., Shin, C. and Marfurt, K. J. (2012), Implementation of elastic-reverse-time migration using wavefield separation in the frequency domain, Geophysical Journal Intern., 189, 1611-1625.

Denli, H., and L. Huang, (2008), Elastic-Wave Reverse-Time Migration with a Wavefield-Separation Imaging Condition, 78th Annual International Meeting, SEG, Expanded Abstracts, 2346-2350.

Du, Q., Zhu, Y., and Ba, J. (2012), Polarity Reversal Correction for Elastic Reverse Time Migration, Geophysics, 77(2), S31-S41.

Huang, L. and M. Albrecht (2011), Seismic and Magneto-Telluric Imaging for Geothermal Exploration at Jemez Pueblo in New Mexico, Proceedings of the Thirty-Sixth Workshop on Geothermal Reservoir Engineering, Stanford University, SGP-TR-191, 944-949.

Huang, L., Kelley, S., Zhang, Z., Rehfeldt, K., Albrecht, M., and Kaufman, G. (2011), Imaging Faults with Reverse-Time Migration for Geothermal Exploration at Jemez Pueblo in New Mexico, GRC Transactions, 35, 833-837.

Kaelin, B., and A. Guitton, (2006), Imaging Condition for Reverse Time Migration, 76th Annual International Meeting, SEG, Expanded Abstracts, 2594-2598.

Liu, F., Zhang, G., Morton, S. A., and Leveille, J. P. (2011), An Effective Imaging Condition for Reverse-Time Migration Using Wavefield Decomposition, Geophysics, 76(1), S29-S39.

McMechan, G. A., (1983), Migration by Extrapolation Of Time-Dependent Boundary Values, Geophysical Prospecting, 31, 413-420. Mulder, W. A., and R.-E. Plessix, (2004), A Comparison between One-Way and Two-Way Wave-Equation Migration, Geophysics, 69, 1491-1504.

Whitmore, N. D., (1983), Iterative Depth Migration by Backward Time Propagation, 53rd Annual International Meeting, SEG, Expanded Abstracts, 382-385.

Yan, J., and Sava, P. (2008), Isotropic Angle-Domain Elastic Reverse-Time Migration, Geophysics, 73(6), S229-S239.

Yan, R., and X. B. Xie, (2010), A New Angle-Domain Imaging Condition for Elastic Reverse-Time Migration, 80th Annual International Meeting, SEG, Expanded Abstracts, 3181-3186.

Yoon, K., K. Marfurt, and E. W. Starr, (2004), Challenges in Reverse-Time Migration, 74th Annual International Meeting, SEG, Expanded Abstract, 1057-1060.